Soft Matter

PAPER

View Article Online
View Journal | View Issue

Cite this: *Soft Matter*, 2015, **11**, 1303

Sphere to rod transitions in self assembled systems probed using direct force measurement†

Christopher J. Fewkes,[ab] Rico F. Tabor[c] and Raymond R. Dagastine*[abd]

The influence of nanoparticle shape, in particular the sphere to rod transition, on surface forces and consequently the properties of colloidal fluids is an interesting but not well investigated phenomenon. Here, the surface force behaviour of concentrated surfactant solutions containing cetyltrimethylammonium bromide and sodium salicylate with micelle shapes varying from slightly prolate to high aspect ratio rods was measured. Atomic force microscopy (AFM) with both rigid particle and soft droplet probes was used with comparisons and analysis made using the Chan–Dagastine–White model. It is observed that small changes to the micelle shape result in no discernable differences to the surface force behaviour, however, once the micelles are elongated significantly, the long range forces adjust in nature from oscillatory to that of a single attractive force well. This highlights the importance that nanocolloid shape has on the behaviour and properties of emulsions and other colloidal fluids, specifically for emulsion flocculation and handling in systems of rod and worm like micelles.

Received 31st October 2014
Accepted 22nd December 2014

DOI: 10.1039/c4sm02399d

www.rsc.org/softmatter

1 Introduction

Many industrial products are made with or involve the processing of colloidal materials. Understanding the properties and behaviour of colloids is essential for efficient processing. When solutions contain many different colloids of varying shape, size and attributes the bulk properties become more complicated. For example, mixed surfactant systems are used as the basis for a lot of commercial products with many forming wormlike micelle aggregates in solution. Despite this, the behaviour of wormlike micelles in emulsions is not well understood.[1,2]

The behaviour of emulsions is heavily influenced by the interactions of the droplets in solution which are appreciably underpinned by the surface forces between the drops. These surface forces can be measured by various force balance methods depending on the magnitude of the force.[3] While micro-Newton scale forces can be investigated by the surface forces apparatus (SFA), nano-Newton forces are better examined by atomic force microscopy (AFM), with femto-Newton forces using methods such as total internal reflection microscopy (TIRM) and looking at particles under Brownian motion.

Although not exclusive to emulsions, an interesting and well studied class of colloidal interactions are the depletion and structural forces that occur when smaller, often nanometre size, colloids arrange between and affect the interactions of larger colloids. A number of studies have focused on characterising the solution structure of these systems and examining the interaction forces between colloid scale objects in the presence of various nano-colloids including surfactants,[4–14] solid particles,[7,8,10,15–19] polymers,[8,15,20,21] polyelectrolytes,[22] emulsion droplets,[7] and solvent molecules themselves.[23,24] The magnitude of these forces varies significantly and as a result various methods have been used to investigate the phenomena; these include AFM,[4–10,15,16,19–22,24] SFA,[11,23] TIRM,[12,13,18] and thin film balance.[14,17,25–27] The force measurement methods span more than four decades in force magnitude and are reflective of the challenges quantifying these forces. Ultimately, these forces arise as a manifestation of nano-colloid structure in solution where the energy of these interactions is on the scale of thermal energy, k_bT, whereas the depletion forces in these systems can arise from very large osmotic pressures on the energy scale of thousands of k_bT, thus requiring quite diverse force measurement methods to resolve these different aspects where no one method may be sufficient to study these systems.

This paper continues the investigation of structural and depletion forces related specifically to surfactants. Some of the earliest work into this area was by Nikolov and Wasan,[14] who used thin film apparatus to examine the stratification of thin liquid films in micellar solutions and latex particle suspensions.

[a]*Particulate Fluids Processing Centre, The University of Melbourne, Parkville, Victoria, 3010 Australia*

[b]*Department of Chemical and Biomolecular Engineering, The University of Melbourne, Parkville, Victoria, 3010 Australia. E-mail: rrd@unimelb.edu.au; Fax: +61 3 8344 4153; Tel: +61 3 8344 4704*

[c]*School of Chemistry, Monash University, Clayton, Victoria, 3800 Australia. E-mail: Rico.Tabor@monash.edu; Tel: +61 3 990 54558*

[d]*Melbourne Centre for Nanofabrication, Clayton, Victoria, 3168 Australia*

† Electronic supplementary information (ESI) available: Video of droplet profile and disjoining pressure for a structural force and a depletion force. Values for the fitting equations used to model the droplet profiles. See DOI: 10.1039/c4sm02399d

They helped verify the explanation of layer-by-layer thinning of ordered structures of micelles and particles. Subsequent force measurements with SFA by Richetti and Kekicheff[11] were able to directly measure the forces due to structuring micelles and quantify the contributions of concentration and separation. Using TIRM Sober and Walz[13] were able to look at much smaller forces and probe the lower concentration limit of structural forces and the onset of multiple oscillations. McNamee *et al.*[10] extended the study to AFM, investigating the effects of collision velocity on high concentration surfactant. This was eventually extended to the direct measurement of structural forces between drops using AFM by Gromer *et al.*[20] This study, in particular, highlighted that hysteresis and "snap in" can occur as a direct result of interface deformation. This has been theorised to affect stability and flocculation.[6,7,20]

Of particular interest is the way that various structural and depletion forces affect the interactions between droplets in emulsion based fluids. Approaches using thin film balance, while a different configuration with an air–water interface, also provide observations in systems with structural forces. For example, the stability of thin films is strongly influenced by the electric double layer interactions from both the charge on the interface and any nano-colloids resident in the film.[25] Other factors such as polydispersity as well as surfactant and micelle concentration are also important to the behaviour of thin films and effect the nano-colloid structuring.[17] Importantly, structural forces can be used to stabilise otherwise unstable films with small, highly charged nano-colloids offering efficient stabilisation due to their large effective volumes.[27] Attempts to investigate the importance of effective volume compared to hard core volume have often shown that the behaviour depends on the solution ionic strength.[6–8,10,26–29]

Even with the large body of work regarding forces and structuring of spherical micelles or particles in a thin film there is an opportunity to extend this research and thinking into non-spherical objects. The influence of worm like micelles on emulsion interactions is of particular importance due to their prevalence in mixed surfactant systems. Despite this, there is only a limited understanding and experimental investigation into how they mediate droplet interactions.

Previous studies into depletion forces with rigid rods[18] have demonstrated that there is a strong depletion attraction between solid surfaces at close approach related to the restriction of the rotational entropy of the rods. This occurs at distances related to the length of the rods and is separate to the normal depletion energy from excluded volume and packing. Significantly smaller secondary attractive forces can also be observed at farther separations if the concentration is sufficiently high but are orders of magnitude below the main attraction and of an unclear origin. Investigations with soft particles such as viruses[30] have found similar results but with a variation in the onset of depletion forces from bending of the rods. Unlike solid particles or viruses, micelles are not only soft but can deform and reform dynamically from outside stimulus. How this dynamic behaviour affects interactions based on the rotation of the particles has yet to be investigated.

The large hydrophillic head groups and thin hydrophobic tails of surfactant molecules can drive aggregation into complicated structures and phases including micelles, lamellar phases, and sponge phases depending on the concentration. The addition of a binding counterion to the surfactant is another common way to affect the micelle aggregation *via* screening the head group repulsion. This study is focused on investigating micelles of varying profile from spherical up to long rods; in particular the behaviour of short rods in solution is poorly documented. Hexadecyltrimethylammonium bromide (CTAB) and sodium salicylate (NaSal) were chosen as they are form a well studied system with considerable shape differences as well as sufficient sizing and rheological data. This study uses AFM between both rigid surfaces and soft droplet probes to observe the impact of micelle shape on surface forces and the changing physical origins of the observed forces. The two techniques allow us to cover a greater force range and determine more about the system than with a single method.

2 Materials and methods

2.1 Materials

Hexadecyltrimethylammonium bromide (CTAB, ultra grade >99%), sodium salicylate (NaSal, reagent grade >99.5%), and decanethiol were obtained from Sigma-Aldrich (New South Wales, Australia) and used as received. Deionised water (minimum resistivity 18.2 MΩ cm) was taken from a Milli-Q system. Perfluorooctane (PFO, 98%) was obtained from Sigma-Aldrich (New South Wales, Australia) and purified over silica (Florisil, also obtained from Sigma, 100–200 mesh) *via* column chromatography. Glass surfaces were cleaned before use by sequential soaking in 10% Ajax Labware Detergent, 10% nitric acid, and 10% sodium hydroxide for one hour each with deionised water rinses in between. Hydrophobic surfaces were prepared by boiling borosilicate glassware in a covered container of ethanol at 100 °C for a minimum of four hours.[31] Silica particles were obtained from Thermo Particle Size Standards. No adjustments were made to solution pH or ionic strength.

2.2 AFM Measurements

Custom rectangular silicon cantilevers (450 μm × 50 μm × 2 μm) with a gold disk at the far end were used for droplet experiments.[7,32] The cantilevers were submerged in a dilute (1%) solution of decanethiol in ethanol to form self-assembled monolayers of decanethiol on the gold surface to increase the surface hydrophobicity. Silica particles were attached to the tips of v-shaped cantilevers (MLCT, Bruker Instruments, Santa Barabra, CA, USA) using a 30 minute two part epoxy (The Original Super Glue Corporation, CA, USA) and allowed to cure for 24 hours. The attached particles were exposed to low concentration ozone in a ozone cleaner (BioForce Nanosciences, Inc., UV/Ozone ProCleaner Plus) before use. Spring constants were measured using the method of Hutter and Bechhoefer[33] and were in the range of 0.1–0.2 N m^{-1} for the custom cantilevers and 0.02–0.04 N m^{-1} for the MLCT

cantilevers. All experiments were performed on an Asylum MFP-3D AFM. A more detailed description of this procedure can be found here.[34] Droplet radii were measured *via* optical microscope. Droplets were formed *via* spray injection using a hypodermic needle submerged in water, before settling onto and self adhering to the silica surface. During the experiment a droplet of desired size was selected and attached to the cantilever by pressing the cantilever onto the drop then pulling it off the surface. Raw data was recorded as photodiode voltage *versus* linear variable differential transformer (LVDT) position. Scan speeds for pseudostatic measurements varied from 50 nm s^{-1} down to 3 nm s^{-1} depending on the viscosity of the solution. The solutions were heated to 50 °C during preparation and allowed to equilibrate to room temperature overnight. The temperature of each experiment was maintained between 25 °C and 27 °C by the use of a room thermostat and the room's temperature controls.

2.3 Interfacial tension and contact angles

Oil–water interfacial tensions were measured using pendant drop tensiometry with a Dataphysics (Germany) OCA20 tensiometer. A pendant drop of PFO was generated in a clear quartz cell containing the CTAB solution. The proprietary instrument software was then used to photograph the drop and fit it to the Young–Laplace equation, providing the interfacial tension. This value was tracked over time until it was considered to be stable, about 10 to 20 minutes. The interfacial tension for PFO in 80 mM CTAB was measured as 13 mN m^{-1}. Contact angles were also measured using the Dataphysics OCA20 tensiometer. A single drop was generated in aqueous solution as described previously and deposited onto a hydrophobic surface at the bottom of the cell. The drop was then photographed and the contact angle measured. The value for PFO in 80 mM CTAB on a hydrophobic silica surface was measured as 135°. Temperature control was not present during this procedure but the solution was heated to 30 °C immediately before the experiment and likely cooled slightly during the measurement.

2.4 Modelling

In direct force measurements between rigid surfaces the determination of surface separation is achieved using the constant compliance region where the two surfaces are in contact; as this region of contact does not commonly occur between drops in an AFM measurement, due to interfacial deformation, a more detailed analysis is required. We use the well established model developed by Chan–Dagastine–White (CDW)[35–39] to quantify the contributions and relative importance of changes in drop separation, deformation, and surface forces on the AFM force data. This model is based on balancing the surfaces forces that cause local deformation to the drop with the overall Laplace pressure of the drops due to their curvature. This is achieved by describing the interfacial deformation using a form of the Young–Laplace equation that accounts for local curvature and deformation as well as surface forces. This interfacial profile and intervening pressure profile between the drops is then used to calculate the same force measured in the AFM. A schematic of the geometry for the AFM as well as the reference frame for the CDW model is shown in Fig. 1.

To calculate a theoretical AFM force profile using the CDW model requires a description of the surface forces in the drop experiments in the form of a disjoining pressure between two flat infinite half spaces. For many systems including van der Waals forces,[34,38,40] electrical double layer forces[39,41–43] and even steric forces,[32] this can be derived from quantitative colloidal theories. For systems where closed form analytic descriptions of the surface forces are difficult to achieve, for example structural forces from spherical nano-colloids in solution, the disjoining pressures have been constructed by using an experimental AFM force measurement between rigid surfaces. A functional form is fitted to the rigid data and then scaled using the Derjagiuin approximation to that of a disjoining pressure between flat surfaces. This approach is less rigorous as the surface chemistry of the rigid interface differs from that of a drop but in the case of drops, the surfaces never come into contact and the structure in solution tends to dominate the surface forces as the drops rarely sample the small separations where the drop surface chemistry impacts on the surface force. This approach has been used to describe the force measurements between drops with a high degree of accuracy.[6,7]

An established semi-empirical equation for spherical nano-colloids in solutions was initially fitted to the rigid data:[44]

$$\frac{F}{R} = 2\pi A \exp\left(\frac{-h}{\varepsilon}\right)\cos\left(\frac{2\pi h}{\lambda} + \phi\right) + c \qquad (1)$$

where F is the force, R is the radius of the particle, and h is the separation between the particle and the surface. The remaining symbols are fitting parameters with A for the amplitude of the oscillations, λ for the periodicity of the oscillations, ε for the decay length of the oscillations, ϕ for the phase lag of the oscillations, and c to account for any force offset. This equation has been used previously for micelle systems, nanoparticles and microemulsions[7] and is explained in more detail elsewhere.[19,44]

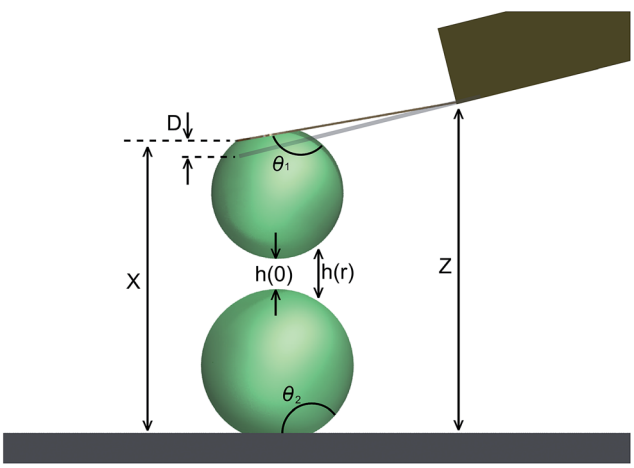

Fig. 1 Diagram of experimental setup during an AFM experiment between two drops, where Z is piezo position, D is cantilever deflection, X is effective end to end drop separation, $h(r)$ is drop separation at radial position r, and θ is contact angle.

For solutions where this equation was unable to provide an agreeable fit an empirical equation was instead used, adding a second decaying oscillation to the above model:

$$\frac{F}{R} = 2\pi A_1 \exp\left(\frac{-h}{\varepsilon_1}\right)\cos\left(\frac{2\pi h}{\lambda_1} + \phi_1\right) + 2\pi A_2 \exp\left(\frac{-h}{\varepsilon_2}\right)\cos\left(\frac{2\pi h}{\lambda_2} + \phi_2\right) + c \quad (2)$$

this model is effective as an empirical fit to the data that was then scaled for use as a disjoining pressure, but caution should be used in assigning a physical significance to the individual model parameters.

3 Results and discussion

3.1 Structural forces in pure CTAB micelles

To investigate the effects of micelle aspect ratio on structural force behaviour a range of micelle aspect ratios were examined. Ideally this would cover ratios from one up to very large values, however, CTAB has been observed to form slightly ellipsoidal micelles even at low concentrations[45] where the aspect ratio and non-spherical behaviour increase with concentration. As such, it was not possible to observe perfectly spherical micelles in solution at a sufficient concentration to observe structural forces. A surfactant solution of 80 mM CTAB was chosen to balance the range of observed aspect ratios with the ability to clearly measure the structural forces of the solution.

A previous study with anionic micelles[7] has shown that moderately ellipsoidal micelles can be treated as effectively spherical. As such, it is our expectation that pure CTAB solutions and solutions of low aspect ratio micelles will show behaviour consistent with rigid spherical nanoparticles.

3.1.1 Deformable interfaces. Fig. 2a shows a plot of the approach and retract force profiles in an 80 mM CTAB solution between two immobilized PFO drops. This curve shows three distinct repulsive regions, with two jumps due to the mechanical instability of the cantilever in an attractive force field during both approach and retract. These regions are typically due to oscillatory sections of the structural force combined with the deformable nature of the drops. The force ramps are attributed to the drops deforming while maintaining the separation and number of micelle layers between them. The characteristic "jump-in(out)" behaviour is attributed to the number of micelle layers between the drops rapidly decreasing(increasing). This behaviour has been seen previously with spherical particles between deformable interfaces.[6,7,20] It should be emphasised that the jumps and hysteresis of the force curve are due to deformations of the droplet surface and are not caused by hydrodynamic drainage forces or coalescence of the interfaces.

Previously, for solutions of anionic micelles, quantitative modelling has shown the presence of additional layers of micelles in the film between the drops that require more force to expel and, although not apparent from the results, some layers cannot be expelled due to the drops deforming. A similar behaviour is expected in the case for CTAB and will be discussed in the modelling discussion below.

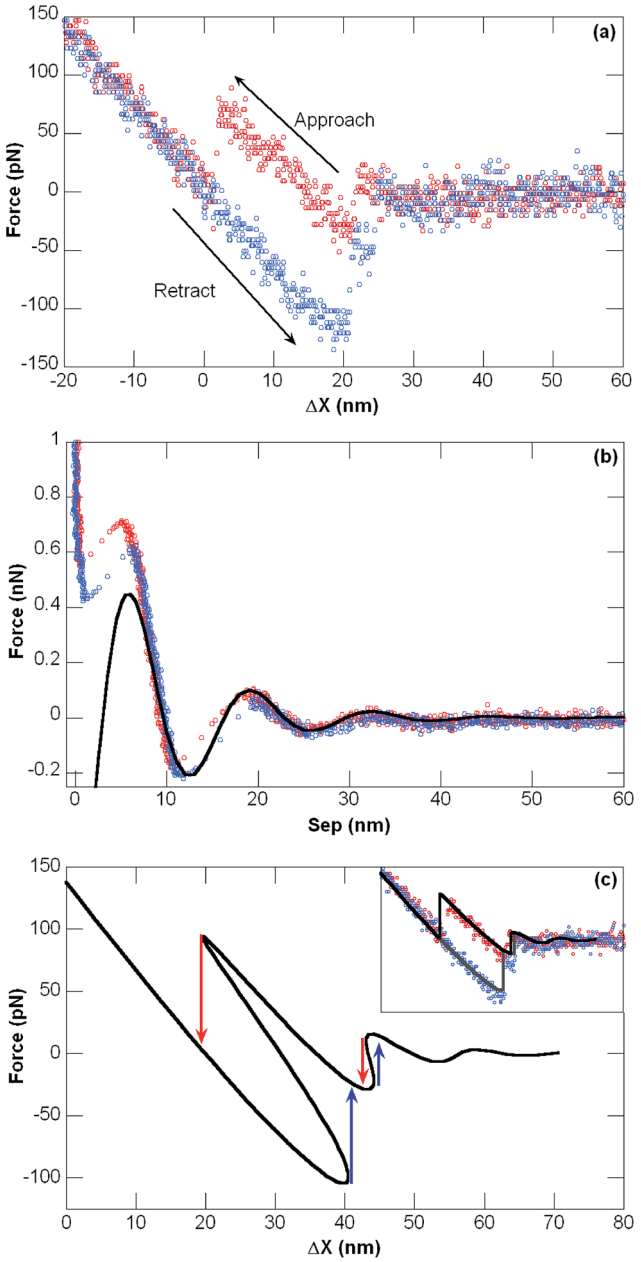

Fig. 2 (a) Interaction forces between two perfluorooctane droplets (diameters 61 and 63 μm) in solution of 80 mM CTAB at 27 °C. Symbols are experimental AFM data for approach (red) and retract (blue). (b) Interaction forces for 80 mM CTAB at 27 °C between a rigid silica particle (radius 7 μm) and a silica surface. The solid black line is a fit using the semi-empirical equation described previously. (c) Modelling results for two perfluorooctane droplets (diameters 61 and 63 μm) calculated by the Chan–Dagastine–White model using the fit to the solution forces in (b). Inset: Model overlayed onto AFM data from (a) with considerations for jump ins and jump outs taken from data.

3.1.2 Rigid Interfaces. Fig. 2b shows force *versus* separation for 80 mM CTAB between rigid surfaces on approach and retract showing typical oscillatory structural force behaviour due to variations in osmotic pressure at different separations. This has been seen previously with similar systems,[7,10] including CTAB.[4] The fitted equation overlayed onto to the data was able to match

most oscillations but deviated at close separations, most likely because the semi-empirical fit does not capture the details of electrical double layer repulsion or surface adsorption. CTAB is known to form a bilayer on silica surfaces[46,47] in a similar manner to the adsorption on mica[48] but behaves differently at the oil–water interface, where only monolayer coverage of the drop interface is expected. As the deformation of the interface limits the separation between drops, it is not expected that the discrepancies between the fitted equation and data for these smaller separations will impact model accuracy in describing the deformable force measurements between drops.

3.1.3 Modelling of disjoining pressure. Fig. 2c shows the predicted equilibrium force profile in 80 mM CTAB solution between two PFO drops with the same droplet radii as the deformable experiment using the disjoining pressure extracted from the rigid data. The arrows indicate where non equilibrium points would occur in the experimental data due to the mechanical instability of the cantilever in an attractive force field; the red arrows indicate jump-ins and the blue arrows indicate jump-outs.

The predicted curve and the experimental data show good agreement. From the model we can determine features that are not explicitly apparent from the experimental data. Of note is that each jump corresponds to the change of a single micelle layer between the drops. Previous studies have shown jumps across multiple layers[6] and our modelling indicates that had our drops been slightly larger, about 80 μm diameter, there would be a single jump out across two layers in this solution also.

Additionally, two remaining micelle layers are present at close approach and cannot be removed even with additional force. This is discussed further in Section 3.5. From this we observe that the deformable experimental data is showing features, corresponding to separations with five micelle layers between the drops, that are obscured below the noise band on the rigid data. This can be explained as the smoothness and increased size of the drops over the solid particles allowing for a greater sensitivity to solution structuring[34] as well as the increase in interaction area due to interfacial deformation. For this reason, deformable systems were primarily chosen to investigate the change in solution structure.

3.2 Elongating the CTAB micelles

To increase the aspect ratio of the CTAB micelles, NaSal was added to the solution in varying concentrations. The Sal^- ions have been shown to locate themselves close to the head groups within the micelles, screening the charge and increasing the molecular packing and number of surfactant monomer units within a micelle.[49] NaSal is preferred over inorganic salts (NaCl, NaBr *etc.*) as the strong binding to the micelles allows for shape changes to be observed at much lower salt concentrations.[51] This allowed us to track the forces over the gradual change in micelle shape from ellipsoidal to short rod to long rod with minimal salt addition. Experiments were conducted at 80 mM CTAB with NaSal concentrations ranging from 0 to 24 mM. The limit of NaSal addition was dependent on the viscosity of the solution; at higher NaSal concentrations the solution was too viscous to satisfactorily measure force curves using drops and may be forming surfactant networks rather than discrete particles.[52] Additionally these solutions would gel at room temperature resulting in difficulty setting up the experiment.

In addition to the increase in aspect ratio, a number of other micelle and solution properties change with the addition of NaSal, as shown in Table 1. One should note that the extrapolations in Table 1 include some uncertainty to the exact aspect ratio and aggregation number values, but the overall trends shown with increasing NaSal or CTAB concentration should persist. The most obvious is that the increased ionic strength of the solution will decrease the length over which electrostatic forces are observed. Additionally, as aggregation increases, the same number of surfactant molecules must now form fewer micelles. Lastly the counterions bound to the micelle surface decrease the surface charge and surface potential. Combined with the decrease in Debye screening length, these effects will reduce the repulsion between micelles and consequently the effective volume of the micelles and thus the magnitude of any structural forces. Given the change in screening length is small compared to the size of the micelle it is believed that this is only

Table 1 Aggregation and size estimations for CTAB micelles with varying CTAB and NaSal concentrations at 26 °C

[CTAB] (mM)	[NaSal] (mM)	Aggregation number[a]	$L/2^a$ (r_2, Å)	Axial ratio r_2/r_1	κ^{-1} (nm)	[Micelle][b] (μM)
80	0	190	50	1.9	3.06	416
80	4.0	236	62	2.3	2.87	337
80	8.0	312	75	2.8	2.70	255
80	12	370	93	3.5	2.56	215
80	16	442	114	4.3	2.44	180
80	20	590	139	5.3	2.33	135
80	24	706	171	6.4	2.23	113
100	0	211	56	2.1	2.74	470
100	20	486	120	4.5	2.19	205
120	24	538	132	5.0	1.96	222

[a] Micelle aggregation numbers and long axis values were estimated by extrapolating from data in Goyal and Dasannacharya[49] using correlations suggested in Das, Cao, Kaiser, Warren, Gladden and Sokol[50] to account for temperature and concentration differences. Micelle short axis taken as 26.5 Å from Goyal and Dasannacharya.[49] [b] CMC for CTAB extrapolated from data in Howard and Craig.[47]

a minor reinforcing effect in this case. Additionally, the polydispersity of the solutions may change with concentration and surfactant/salt ratio, but this is not expected to be sufficient to alter packing structure.

3.2.1 Deformable interfaces. Deformable interfaces were used to investigate any changes in solution structure and highlight key differences and points of interest. Fig. 3 shows various force profiles on approach and retraction between PFO drop pairs for CTAB with added NaSal amounts increasing from left to right. The increasing salt concentration elongates the micelles and results in changes to the force profiles. It is important to mention that the experiments were performed on different droplet pairs with different radii. This makes comparing fine details difficult as there is an effect on force magnitudes and behaviour based on the droplet size. Unfortunately this effect is nonlinear with droplet size[34] and cannot be easily removed from the analysis.

At low NaSal concentrations, 80 mM CTAB/4 mM NaSaI (80/4) and 80 mM CTAB/8 mM NaSaI (80/8), the force profiles are not significantly different from that for a structural force from spherical micelles. This is consistent with the aforementioned study[7] where force measurements for slightly prolate SDS micelles still demonstrated significant structuring. Compared to previous studies with SDS micelles, this data shows that to affect the interaction forces through changes in solution structure a moderate change in aspect ratio must be achieved.

Increasing the NaSal concentration to 12 mM changes the force profile and results in behaviour that is not perfectly explained by a standard structural force. The main difference is the increase in the peak attractive force on retract from between 100 and 200 pN to over 400 pN. This is a considerable increase and highlights a significant difference in the attractive force at minimum separation. Additionally, on approach, the second repulsive 'ramp' has decreased in peak repulsive force and the subsequent jump in is to a larger attractive force.

Increasing the NaSal concentration to 16 mM has the effect of removing the repulsive ramp from the force curve entirely on approach. This has significant implications for the behaviour of droplets in solution, especially regarding emulsion stability and flocculation, as they no longer experience a repulsive force before they are close enough to experience a strong attractive force. A small kink or step is observed in the curve during jump in and may indicate a small region of stable separation between close contact and the point where depletion attraction begins. Although the kink was reproducible, it varied in both size and angle on the force curve throughout an individual experiment. This kink is not expected if the behaviour was determined purely by depletion forces. The actual separation of the drops is not obvious from the force profile and requires additional analysis.

Further addition of NaSal to 20 then 24 mM only appears to change the force behaviour in subtle ways. The only significant change is the loss of the kink and increase in sharpness of the jump in. The magnitude of the attractive force on retraction differs but only within the normal variation typical for these measurements. At (80/24) the force profile matches the expected shape of a pure depletion force.

3.2.2 Rigid interfaces. To investigate the loss of the repulsive maximum and the transition in long range forces from oscillatory to attractive, the force profiles of (80/12) and (80/16) were measured using rigid particles, shown in Fig. 4a. These force curves show the same increase in the depth of the attractive force well compared to (80/0), and also highlight a decrease in the solution structuring at larger separations not apparent from the deformable curves. Additionally we can see that the transition from oscillatory to attractive is matched with the rigid data with the significant reduction in the repulsive force maximum of (80/16) compared to (80/12).

3.2.3 Modelling of disjoining pressure. The changes in force behaviour of the rigid data with the solution structure are generally consistent, but to quantitatively correlate the observations of the forces between rigid interfaces with force measurements between deformable interactions, the rigid force data was used in the deformable model to predict the observed force behaviour and compared to the experimental observations including the unusual step in behaviour observed. When

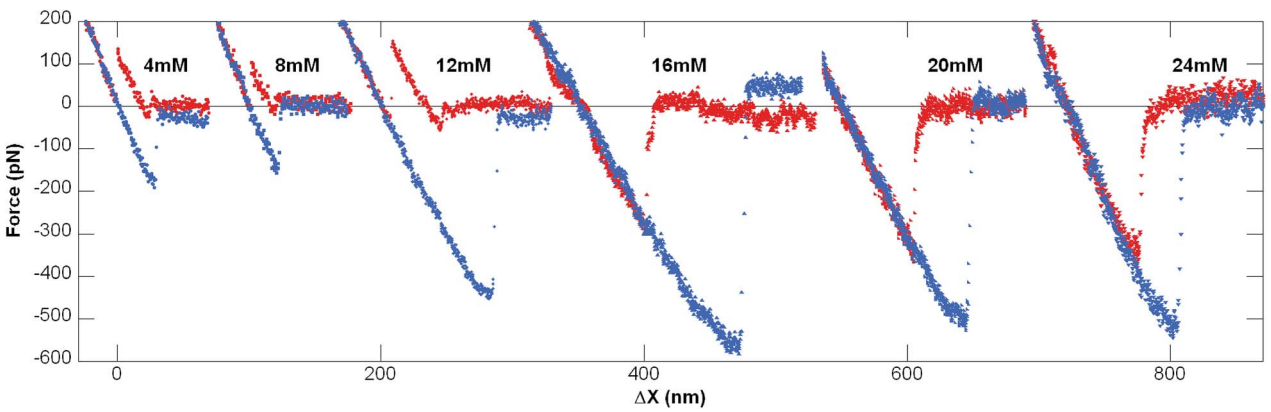

Fig. 3 Interaction forces between two perfluorooctane droplets in 80 mM CTAB solutions with increasing amounts of NaSal at 26 °C. Plots offset horizontally for convenience. From left to right the solutions are: 4 mM NaSal, droplet diameters are 71 and 72 μm, 26 °C; 8 mM NaSal, droplet diameters are 75 and 78 μm; 12 mM NaSal, droplet diameters are 72 and 83 μm; 16 mM NaSal, droplet diameters are 72 and 75 μm; 20 mM NaSal, droplet diameters are 72 and 82 μm; 24 mM NaSal, droplet diameters are 71 and 69 μm.

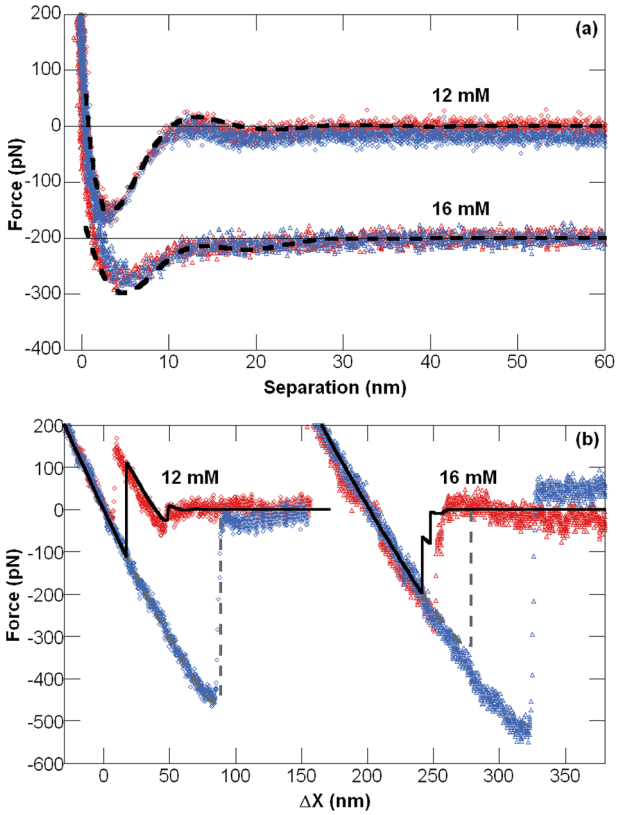

Fig. 4 (a) Force *versus* separation data between a rigid silica particle (radius 4 μm) and a silica surface in 80 mM CTAB with 12 mM NaSal at 25 °C and 16 mM NaSal at 25 °C. Symbols are AFM data for approach (red) and retract (blue). The dashed black lines are fits using the semi-empirical equation described previously. (b) Modelling results using the fits to the rigid data calculated by the Chan–Dagastine–White model overlayed onto AFM data from Fig. 2 with considerations for jump ins and jump outs taken from data. The solid lines are the expected behaviour for approach (solid black) and retract (dashed grey).

attempting to fit a profile to the rigid data it was found that these concentrations cannot be successfully modelled using the semi-empirical equation for the spherical micelles. Instead a purely empirical equation, see Section 2.4, was used to match the general shape of the force profiles. The parameters were adjusted to match the deformable data within the range of the rigid experiments. This equation accurately captured the experimental observations between rigid interfaces into a simple form that was scaled to construct a disjoining pressure in the deformable model calculation, although the parameters within this model were not found to have any physical significance beyond curve fitting.

Fig. 4b shows the model predictions overlayed onto the deformable data. Good agreement was achieved for (80/12) with all observed features matching and only slight magnitude differences observed. The (80/16) solution is able to predict the step in, which occurs due to the local force maximum at 13 nm separation on the rigid curve, but is unable to perfectly match the position of the step in or the position and magnitude of the jump out. Although these differences could be due to obscuration from partial surface adsorption or roughness in the rigid experiment, it may be as a result of differences between the oil–water and silica–water interfaces. It is important to note that the modelling indicates that no micelle layers are present at close separation between the oil drops in either of these solutions. Given that coalescence was not observed, this indicates that other forces are stabilising the droplets. This is most likely due to the saturated monolayer coating of surfactant on the drops providing electrical double layer repulsion and potentially steric repulsion at high solution ionic strengths. This close approach is necessary for the drops to experience the full magnitude of the depletion well.

It is also interesting to note that the finer features of the deformable force curves, such as the small step in for (80/16), can be predicted using the CDW model. Such features are due to a combination of small repulsive maxima and the drops ability to deform to different separation 'layers' at different radial positions. Of interest is that there are two force minima within the depletion zone in the rigid (80/16) curve: a faint dip starting at 30 nm separation and a strong well at separations less than 10 nm. This behaviour is fascinating and again appears to be interplay between the wanning structural force and the increase of the rotational entropic force from the rod like micelles. It should be mentioned that the attractive osmotic force from exclusion of all particles between the surfaces is still present for rod micelles and it is the decrease in magnitude and number of observable oscillations beyond this that is that is the key change of the structural force. The features of the disjoining pressure required to create this force profile are just visible within the noise of the rigid (80/16) data, but clearly visible as the small oscillation and kink in the deformable measurements.

3.3 Rod CTAB micelles

As mentioned previously, the (80/24) solution exhibits purely depletion behaviour. To further explore the force behaviour in what appears to be a depletion dominated force regime we measured the solution behaviour between rigid interfaces. This was subsequently compared with the deformable measurements using the modelling described previously.

As seen in Fig. 5a the rigid force curve for (80/24) shows a single attractive depletion well beginning at a distance roughly 30 nm from close approach. This distance is well beyond the estimated diameter of the micelles and may instead be indicative of the effective micelle length from the micelle long axis. An empirical model, based on the decaying oscillations used in the structural model, has been fitted to the experimental data.

The expected deformable force curve based on the modelling is overlayed onto the experimental force curve in Fig. 5b. The theory curve successfully matches the general shape of the force curve and although the point of jump in and jump out are underestimated by as much as 30 nanometres. This difference may reflect the complex adsorption characteristics of the different interfaces within the system. The theoretical force curve does not account for differences in electrical double layer forces from the different interfaces. The oil–water interfaces are expected to contain monolayers whereas the silica water interfaces are expected to contain bi-layers, and will thus differ in the

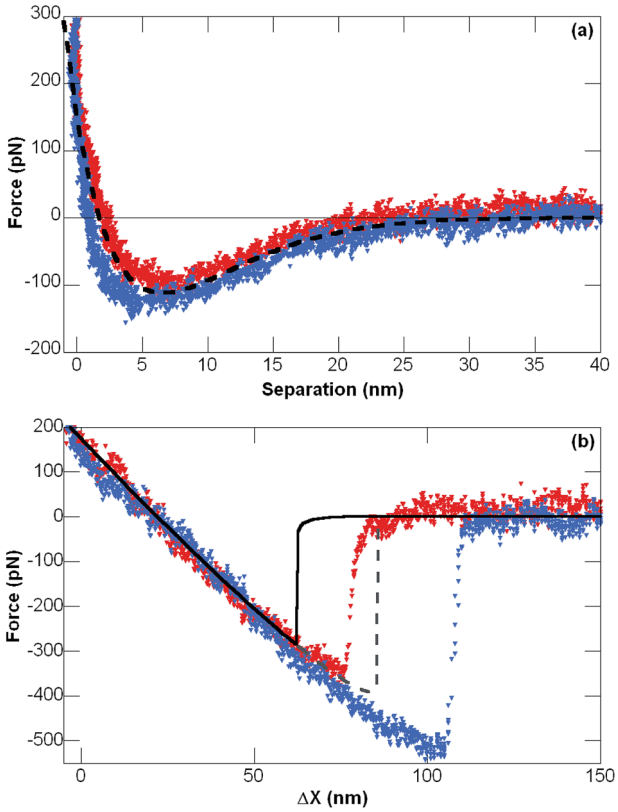

Fig. 5 (a) Force *versus* separation data between a rigid silica particle (radius 4 μm) and a silica surface in 80 mM CTAB with 24 mM NaSal at 25 °C. Symbols are AFM data for approach (red) and retract (blue). The dashed black line is a fit using the semi-empirical equation described previously. (b) Modelling results using the fit to the rigid data calculated by the Chan–Dagastine–White model overlayed onto AFM data from Fig. 2 with considerations for jump ins and jump outs taken from data. The solid lines are the expected behaviour for approach (solid black) and retract (dashed grey).

surface charge and consequently the magnitude of repulsive forces at close range. Additionally the relatively lower number density than previous solutions, see Table 1, reduces the sensitivity to subtle features, especially for the rigid experiment, and may simply prevent the onset of depletion from being accurately measured.

3.4 Increase in concentration

In the previous experiments, as the micelles elongated the number of micelles decreased, reducing the overall magnitude of observable forces and making it difficult to investigate the interplay between the various phenomena. To further investigate this subtle feature both rigid and deformable data was taken for solutions at the same CTAB/NaSal ratio as the (80/16) solution, but at increased concentrations. This allows us to look at the effect of both micelle rod length and number density in solutions where both osmotic and rotational entropy forces are present. Shown in Table 1, increasing the concentration from (80/16) to (100/20) and (120/24) allows us to observe the change from an increase in rod length and micelle number density. Based on our expected micelle sizes and trends, the change from (80/16) to (100/20) is primarily from the change in number density but the change from (100/20) to (120/24) includes both effects. Additionally (120/24) can also be compared to (80/20) as the micelles are of similar length but at a much higher number density.

The rigid force *versus* separation profiles for (100/20) and (120/24), shown in Fig. 6a, both demonstrate a large depletion zone at close separation but differ in the presence of a local maximum within the depletion region. The (100/20) solution has a distinct local maximum around 15 nm separation but as the aspect ratio increases for the (120/24) solution the apparent structure in the force curve wanes and there is only an upwards inflection at an equivalent point. Compared to the (80/16) solution shown in Fig. 4, these repulsive points are more apparent, most likely due to the increase in micelle number density, but at the same time located at a more attractive force; an observation consistent with an increase in both structural

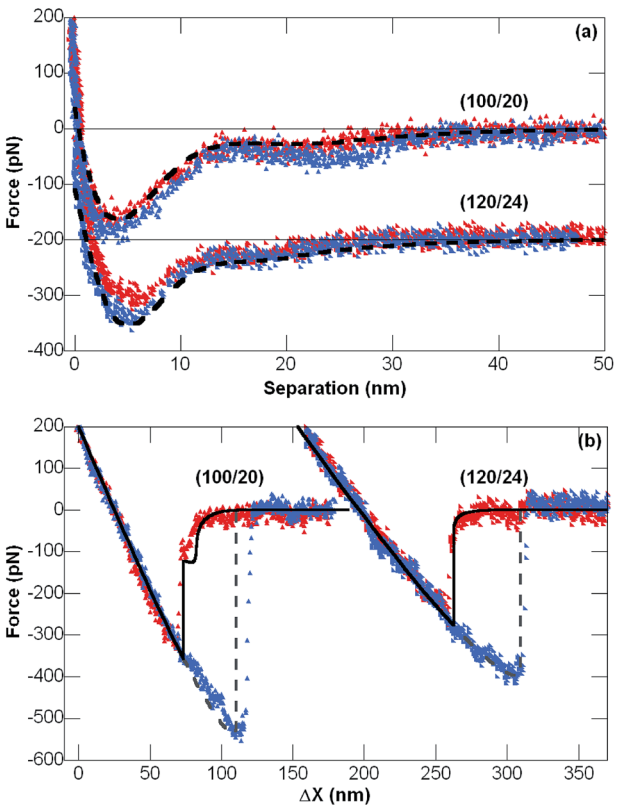

Fig. 6 (a) Force *versus* separation data between a rigid silica particle (radius 4 μm) and a silica surface in 100 mM CTAB with 20 mM NaSal at 25 °C and 120 mM CTAB with 24 mM NaSal at 25 °C. Symbols are AFM data for approach (red) and retract (blue). The dashed black lines are fits using the semi-empirical equation described previously. (b) Force *versus* separation data between PFO droplets in 100 mM CTAB 20 mM NaSal, droplet diameters are 72 and 66 μm, 25 °C and 120 mM CTAB 24 mM NaSal, droplet diameters are 69 and 72 μm, 25 °C. Modelling results using the fits to the rigid data calculated by the Chan–Dagastine–White model are overlayed with considerations for jump ins and jump outs taken from data. The solid lines are the expected behaviour for approach (solid black) and retract (dashed grey).

and depletion forces. These weak oscillations are theorised to be due to structuring of the micelles within the depletion zone. It is unknown if it is from alignment of the micelles along their short axis or from exclusion of the micelles based on their time averaged radius of rotation. Answering this will require accurate sizing of the micelles and knowledge of the effective length of electrostatic forces, both of which are outside the scope of this paper.

Fig. 6b shows the deformable data for these solutions and shows behaviour that can be expected given their respective rigid profiles. Similar to the deformable curves for (80/16) and (80/20) both are purely attractive but without the 'clean' jump expected of a pure depletion force shown with (80/24). Additionally the difference between these two curves mirrors the eventual disappearance of the secondary structure in the depletion well, from (80/16) to (80/20). The (100/20) solution can be compared to the (80/16) solution where the AR is quite similar, but the number density is less for the (80/16) case. Both instances show a large attractive well and a small kink on the way in where the kink is more pronounced for the higher number density, (100/20). The (120/24) solution has a single jump in without any intermediate step but slopes in initially before the jump in similarly to the (80/20) solution, which also has a larger AR. Additionally the magnitudes of jump-in for (120/24) and (80/20) are similar despite differences in surfactant concentration and number density. This is interesting as it demonstrates that the behaviour of droplets may be primarily related to the shape of the micelles and not their number density.

As with the (80/16) solution, empirical modelling was fit to both rigid and deformable profiles with good agreement found between the curves. The agreement in magnitude for jump in and jump out between the curves indicates the disagreement for (80/16) may not be solution related. Attempting to tailor the disjoining pressure profile of (100/20) to exactly fit the observable kink proved to be difficult, as any small change to the local maximum would result in significant differences to the observed kink during jump in. This difference highlights the sensitivity of the drops to changes in the force profile and the importance of the secondary repulsive maximum in determining any semi-stable separations.

Although the above results are for a cationic surfactant with a binding anion, the observed behaviour should be applicable for anionic surfactants shown to exhibit structural forces in solution and a transition from spheres to rods. Multiple studies have demonstrated that the effective length scales for structural and depletion forces at moderate ionic strengths are greater than the physical micelle size.[26–29] We hypothesise that it is the arrangement and packing of the effective micelle shape and disruption to regular packing and layering that determines the transition from structural force to depletion forces. As such, the behaviour and packing structure of any non-spherical object will be connected to conditions that affect electrostatic repulsion.

Surfactants with the same head group as CTAB but with different chain lengths may provide insight into this phenomenon. The length of the hydrophobic tail influences the size of the micelle with shorter tails generally forming smaller micelles.[53] With a smaller micelle radius we speculate that a higher aspect ratio but shorter total length will be required to see the same transition given the additional size from electric double layer repulsion. This also applies to other micellar systems such as SDS with cationic hydrotropic salt[54] where differences in micelle ionisation fraction may further change the required hard micelle shape required to achieve the same effective aspect ratio.

3.5 Discussion of droplet profiles

For the case of a pure structural force and depletion force, we have compared the CDW model calculation to the force data and observed reasonable agreement. For the CDW model to predict the AFM force data accurately, an implicit interfacial force profile between the drops is required for each force data point used in the model.

Fig. 7 shows sample interfacial profiles extracted from the CDW calculation with the disjoining pressure on the drop displayed as an inset for a single point on an AFM force plot. A series of profiles can be viewed as a movie and is available in the ESI.† At large separations the drops are beyond the range of

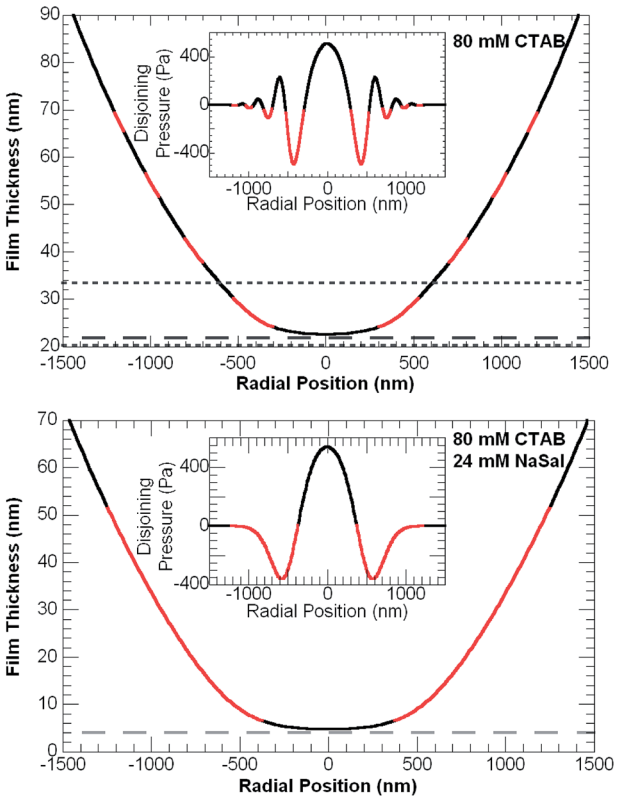

Fig. 7 Thin film profiles between drops as a function of radial position taken from the calculated profiles for a structural force based on the solution of 80 mM CTAB and a depletion force based on the 80 mM CTAB 24 mM NaSal solution. Red lines indicate separations with attractive disjoining pressure. Dotted lines indicate regions of maximum pressure. Dashed lines indicate minimum separation between the droplets.

strong surface forces and do not deform significantly. When the separation is at a position of strong disjoining pressure the local drop interfaces deform by flattening away from contact if repulsive and deforming towards contact if attractive. If the repulsive pressure exceeds the Laplace pressure of the drop, the interface will continue to flatten even at high forces and the film will not thin below a minimum film thickness, of the order of 5 to 30 nanometres depending on the surface forces, geometry of the drops, and interfacial tension. It is important to point out the scale of the drop deformation is only nanometres over a radius of hundreds of nanometres for a 50–100 micrometre diameter drop.

The main feature of the (80/0) solution, the oscillating regions of attractive and repulsive pressure, results in interesting behaviour of the film. As a function of radial position, the local interaction force on the drops is changing from repulsive to attractive. Under these conditions this can result in inflection points in the interfacial profile. Additionally these variations combined with the constant drop volume constraint results in the profile forming a 'pimple'[37] where the film is disproportionately closer in the centre than at farther radial positions. This can be observed in the movie shown in the ESI.†

The profiles for the depletion case, based on (80/24), show different behaviour. As the pressure is attractive except at close separations the drop does not show any inflection points. A video of the profiles is also available in the ESI.†

3.6 Dynamic force curves

Fig. 8 shows the effect of hydrodynamic drainage on the interactions and solution structure for both rigid and deformable force curves for (80/0) and (80/16). As expected, increasing the collision speed within an experiment increases the hydrodynamic film drainage forces for that experiment.[32] For all solutions tested, increasing the velocity reduces how prevailing the structural/depletion forces are to the overall curve. Despite this, the structure is still apparent even to moderate speeds where hydrodynamics is prevailing. The deformable curves in particular still show remnants of the final jump in up until the hydrodynamic drainage forces completely dominate the force curve. This fits with previous observations that solution structure is additive to hydrodynamic drainage forces[16] and is not significantly disrupted by fluid flow at these relatively low velocities.

It is also important to note that the increase in collision velocity is one factor increasing the hydrodynamic drainage force, but solution viscosity changes with micelle shape will also affect these forces. Comparing (80/16) to (80/0) there is a significant increase in hydrodynamic drainage forces seen as an increase in hysteresis at a given speed. This is easily observed

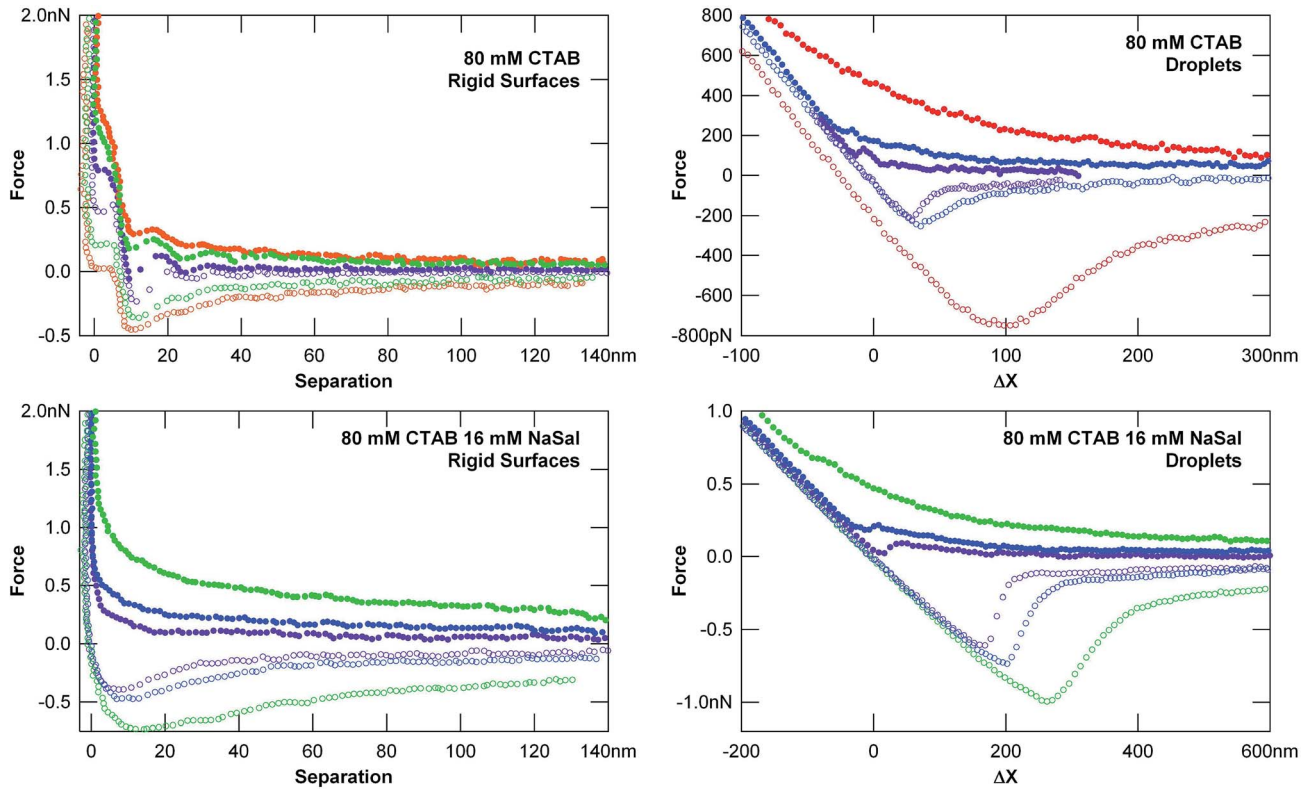

Fig. 8 Interaction forces between a silica particle (7 μm radius) and silica surface in 80 mM CTAB, two perfluorooctane droplets (62 and 63 μm diameter) in 80 mM CTAB, a silica particle (4 μm radius) and silica surface in 80 mM CTAB 16 mM NaSal, and two perfluorooctane droplets (72 and 75 μm diameter) in 80 mM CTAB 16 mM NaSal. Data was smoothed during analysis for clarity purposes. Collision speeds are 1.0 μm s^{-1} (purple), 2.0 μm s^{-1} (blue), 5.0 μm s^{-1} (green), 7.9 μm s^{-1} (orange), and 10 μm s^{-1} (red).

with the 5 μm s^{-1} curves for the rigid experiments; the (80/0) solution only deviates from static forces by about a hundred pico-Newtons but the (80/16) solution difference is on the scale of five to six hundred pico-Newtons. This difference is in agreement with the expected increased viscosity of the solutions shown in literature.[52]

4 Summary and conclusions

The surface forces between deformable and rigid interfaces in solutions of CTAB and NaSal were measured using AFM. The pure CTAB solution showed the typical oscillatory behaviour associated with a structural force indicating the micelles behave like spherical particles. The Chan–Dagastine–White model was used to compare the rigid and deformable measurements through the disjoining pressure between flat plates, constructed from the rigid experiment and the equilibrium force separation drop profiles, providing a prediction of the deformable experiments, with good agreement found.

Elongating the CTAB micelles from spheres to rods resulted in a shift in long range forces from oscillatory to a single attractive well once the micelle shape had been changed significantly. Although the transition was relatively sharp, the surface forces either side of the transition show signs of both structure and depletion. This leads to our suggestion that the transition is the combination of a decrease in osmotic forces and an increase in rotational entropic forces. This behaviour was observed for both rigid and deformable interfaces with a greater level of understanding possible through the combination of the two techniques.

Investigations into the effect of number density found only minimal differences, indicating the bulk of the changes in the force profiles are from the shape change of the micelles. This highlights the importance that the shape of nanocolloids in general has on the behaviour and properties of emulsions and other colloidal fluids. These results specifically have implications for emulsion flocculation and handling in systems of rod and worm like micelles.

Finally experiments conducted at dynamic collision speeds demonstrated the increase in viscosity that occurs from the change in solution. The resulting curves still demonstrated the underlying structural and depletion forces supporting the theory that hydrodynamic drainage, at least at low shear, does not significantly impact particle structuring and may be considered additive to other forces.

Of significant interest is the capacity shown here to easily switch the interactions between droplets using a small addition of the relevant binding counter-ion. The interaction changes from a minimal flocculation well (loosely structured emulsion) with repulsion on approach (*i.e.* an activation limited flocculation) to a deep attractive minimum with no barrier (gelled/flocculated). This has implications on emulsion properties and rheology beyond the immediate change in the properties of the surfactant solution and highlights the importance of a complete understanding at all length scales when trying to understand complex fluids.

Acknowledgements

This work was performed in part at the Melbourne Centre for Nanofabrication (MCN) in the Victorian Node of the Australian National Fabrication Facility (ANFF) and in the Materials Characterisation and Fabrication Platform (MCFP) at the University of Melbourne. We thank the ARC for funding and the PFPC for providing infrastructure support.

Notes and references

1 C. A. Dreiss, *Soft Matter*, 2007, **3**, 956–970.
2 Z. Chu, C. A. Dreiss and Y. Feng, *Chem. Soc. Rev.*, 2013, **42**, 7174–7203.
3 I. Larson and J. Ralston, in *Encyclopedia of Surface and Colloid Science*, ed. A. T. Hubbard and M. Dekker, New York, 2002, vol. 1.
4 G. K. James and J. Y. Walz, *Colloids Surf., A*, 2014, **441**, 406–419.
5 M. Piech and J. Y. Walz, *J. Colloid Interface Sci.*, 2002, **253**, 117–129.
6 R. F. Tabor, D. Y. C. Chan, F. Grieser and R. R. Dagastine, *J. Phys. Chem. Lett.*, 2011, **2**, 434–437.
7 R. F. Tabor, H. Lockie, D. Y. C. Chan, F. Grieser, I. Grillo, K. J. Mutch and R. R. Dagastine, *Soft Matter*, 2011, **7**, 11334–11344.
8 R. von Klitzing, E. Thormann, T. Nylander, D. Langevin and C. Stubenrauch, *Adv. Colloid Interface Sci.*, 2010, **155**, 19–31.
9 C. E. McNamee, Y. Tsujii and M. Matsumoto, *Langmuir*, 2004, **20**, 1791–1798.
10 C. E. McNamee, Y. Tsujii, H. Ohshima and M. Matsumoto, *Langmuir*, 2004, **20**, 1953–1962.
11 P. Richetti and P. Kékicheff, *Phys. Rev. Lett.*, 1992, **68**, 1951–1954.
12 T. D. Iracki, D. J. Beltran-Villegas, S. L. Eichmann and M. A. Bevan, *Langmuir*, 2010, **26**, 18710–18717.
13 D. L. Sober and J. Y. Walz, *Langmuir*, 1995, **11**, 2352–2356.
14 A. D. Nikolov and D. T. Wasan, *J. Colloid Interface Sci.*, 1989, **133**, 1–12.
15 S. Ji and J. Y. Walz, *Langmuir*, 2013, **29**, 15159–15167.
16 A. Tulpar and J. Y. Walz, *Colloids Surf., A*, 2007, **300**, 268–280.
17 D. T. Wasan, A. D. Nikolov and F. Aimetti, *Adv. Colloid Interface Sci.*, 2004, **108–109**, 187–195.
18 L. Helden, G. H. Koenderink, P. Leiderer and C. Bechinger, *Langmuir*, 2004, **20**, 5662–5665.
19 H. L. K. Sabine, G. Stefan, Z. Yan and K. Regine von, *J. Phys.: Condens. Matter*, 2008, **20**, 494232.
20 A. Gromer, R. Penfold, A. P. Gunning, A. R. Kirby and V. J. Morris, *Soft Matter*, 2010, **6**, 3957–3969.
21 A. J. Milling and B. Vincent, *J. Chem. Soc., Faraday Trans.*, 1997, **93**, 3179–3183.
22 A. J. Milling, *J. Phys. Chem.*, 1996, **100**, 8986–8993.
23 R. G. Horn and J. N. Israelachvili, *J. Chem. Phys.*, 1981, **75**, 1400–1411.
24 J. O. S. Sean, *Jpn. J. Appl. Phys.*, 2001, **40**, 4309.
25 D. Exerowa, T. Kolarov, N. E. Esipova, R. Yankov and Z. M. Zorin, *Colloid J.*, 2001, **63**, 45–52.

26 K. D. Danov, E. S. Basheva, P. A. Kralchevsky, K. P. Ananthapadmanabhan and A. Lips, *Adv. Colloid Interface Sci.*, 2011, **168**, 50–70.
27 D. Wasan and A. Nikolov, *Curr. Opin. ColloidInterface Sci.*, 2008, **13**, 128–133.
28 Y. Zeng, S. Grandner, C. L. P. Oliveira, A. F. Thunemann, O. Paris, J. S. Pedersen, S. H. L. Klapp and R. von Klitzing, *Soft Matter*, 2011, **7**, 10899–10909.
29 M. Piech and J. Y. Walz, *Langmuir*, 2000, **16**, 7895–7899.
30 A. W. C. Lau, K.-H. Lin and A. G. Yodh, *Phys. Rev. E: Stat., Nonlinear, Soft Matter Phys.*, 2002, **66**, 020401.
31 S. Biggs and F. Grieser, *J. Colloid Interface Sci.*, 1994, **165**, 425–430.
32 O. Manor, I. U. Vakarelski, X. Tang, S. J. O'Shea, G. W. Stevens, F. Grieser, R. R. Dagastine and D. Y. C. Chan, *Phys. Rev. Lett.*, 2008, **101**, 024501.
33 J. L. Hutter and J. Bechhoefer, *Rev. Sci. Instrum.*, 1993, **64**, 1868–1873.
34 R. F. Tabor, F. Grieser, R. R. Dagastine and D. Y. C. Chan, *J. Colloid Interface Sci.*, 2012, **371**, 1–14.
35 D. Y. C. Chan, R. R. Dagastine and L. R. White, *J. Colloid Interface Sci.*, 2001, **236**, 141–154.
36 D. Y. C. Chan, E. Klaseboer and R. Manica, *Soft Matter*, 2011, **7**, 2235–2264.
37 D. Y. C. Chan, E. Klaseboer and R. Manica, *Adv. Colloid Interface Sci.*, 2011, **165**, 70–90.
38 R. R. Dagastine and L. R. White, *J. Colloid Interface Sci.*, 2002, **247**, 310–320.
39 S. A. Nespolo, D. Y. C. Chan, F. Grieser, P. G. Hartley and G. W. Stevens, *Langmuir*, 2003, **19**, 2124–2133.
40 R. F. Tabor, R. Manica, D. Y. C. Chan, F. Grieser and R. R. Dagastine, *Phys. Rev. Lett.*, 2011, **106**, 064501.
41 R. F. Tabor, A. J. Morfa, F. Grieser, D. Y. C. Chan and R. R. Dagastine, *Langmuir*, 2011, **27**, 6026–6030.
42 R. F. Tabor, C. Wu, H. Lockie, R. Manica, D. Y. C. Chan, F. Grieser and R. R. Dagastine, *Soft Matter*, 2011, **7**, 8977–8983.
43 R. F. Tabor, D. Y. C. Chan, F. Grieser and R. R. Dagastine, *Angew. Chem. Int., Ed.*, 2011, **50**, 3454–3456.
44 S. H. L. Klapp, Y. Zeng, D. Qu and R. von Klitzing, *Phys. Rev. Lett.*, 2008, **100**, 118303.
45 F. Quirion and L. J. Magid, *J. Phys. Chem.*, 1986, **90**, 5435–5441.
46 J. L. Parker, V. V. Yaminsky and P. M. Claesson, *J. Phys. Chem.*, 1993, **97**, 7706–7710.
47 S. C. Howard and V. S. J. Craig, *Langmuir*, 2009, **25**, 13015–13024.
48 W. A. Ducker and E. J. Wanless, *Langmuir*, 1998, **15**, 160–168.
49 P. S. Goyal, B. A. Dasannacharya, V. K. Kelkar, C. Manohar, K. Srinivasa Rao and B. S. Valaulikar, *Phys. B*, 1991, **174**, 196–199.
50 N. C. Das, H. Cao, H. Kaiser, G. T. Warren, J. R. Gladden and P. E. Sokol, *Langmuir*, 2012, **28**, 11962–11968.
51 G. Garg, P. A. Hassan and S. K. Kulshreshtha, *Colloids Surf., A*, 2006, **275**, 161–167.
52 V. Hartmann and R. Cressely, *Colloids Surf., A*, 1997, **121**, 151–162.
53 V. K. Aswal and P. S. Goyal, *Phys. B*, 1998, **245**, 73–80.
54 P. A. Hassan, G. Fritz and E. W. Kaler, *J. Colloid Interface Sci.*, 2003, **257**, 154–162.